Using Nanoscale Substrate Curvature to Control the Dimerization of a Surface-Bound Protein

Martin Kurylowicz, Maximiliano Giuliani, and John R. Dutcher*

Department of Physics, University of Guelph, Guelph ON, Canada N1G 2W1

ABSTRACT The influence of surface geometry on adsorbed proteins offers new possibilities for controlling quaternary structure by manipulating protein–protein interactions at a surface, with applications that are relevant to protein aggregation, fibrillation, ligand binding, and surface catalysis. To understand the effect of surface curvature on the structure of the surface-bound protein β-lactoglobulin (β-LG), we have used a combination of polystyrene (PS) nanoparticles (NPs) and ultrathin PS films to fabricate chemically pure, hydrophobic surfaces that have nanoscale curvature and are stable in aqueous buffer. We have used single molecule force spectroscopy to measure the detachment contour lengths L_c for β-LG adsorbed on the highly curved PS surfaces, and we compare these values *in situ* to those measured for β-LG adsorbed on flat PS surfaces on the same samples. The L_c distributions measured on all flat PS surfaces show a large monomer peak near 60 nm and a smaller dimer peak at 120 nm. For 190 and 100 nm diameter NPs, which are effectively flat on the scale of the β-LG molecules, there is no measurable difference between the L_c distributions obtained for the flat and curved surfaces. However, for 60 nm diameter NPs the dimer peak is smaller, and for 25 nm diameter NPs the dimer peak is absent, indicating that the number of surface-bound dimers is significantly reduced by an increase in the curvature of the underlying surface. These results indicate that surface curvature provides a new method of manipulating protein–protein interactions and controlling the quaternary structure of adsorbed proteins.

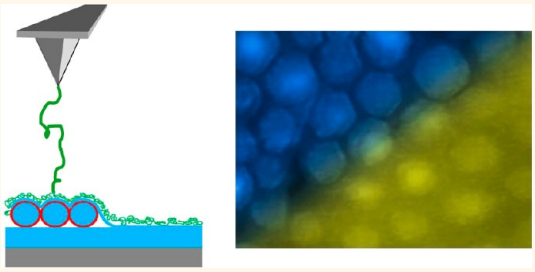

KEYWORDS: protein adsorption · surface curvature · nanoparticles · dimerization · single-molecule force spectroscopy

The emergence of nanotechnology has led to the fabrication of a wide variety of nanostructures such as nanoparticles of various shapes, nanowires, and extended molecules of intricate architecture such as C_{60}.[1] The availability of these nanostructures has made it possible to probe the effect of nanoscale surface geometry on the structure and function of adsorbed proteins. Possible biological applications of biomolecular-nanoparticle conjugates include biosensing,[2,3] drug delivery,[4,5] and the creation of new classes of advanced biomaterials.[6] Just as pH, temperature, pressure, electric field, and other environmental conditions influence the state of proteins and the biological events that they control, surface geometry offers another means of manipulating biomolecular events, and it has the advantage of spatial localization.

A number of studies have demonstrated changes in protein structure and function due to the adsorption of proteins onto NPs of various diameters. Most of these investigations have used optical spectroscopy techniques to measure colloidal suspensions of protein-coated NPs with diameters less than ~100 nm, including Trp fluorescence,[7,8] CD,[9–12] UV–vis,[10,13,14] IR,[8,10,15] and SPR[13,16,17] spectroscopies. These studies have used NPs of a wide variety of materials and diameters. Gold NPs have been used to study BSA,[16,17] cytochrome *c*,[10] and Aβ protein.[14] A study of Aβ42 on various oxide NPs found that TiO_2 promoted the formation of β-amyloid fibrils, whereas other oxides, such as SiO, ZrO_2, and CeO_2, and fullerenes C_{60} and C_{70} did not.[18] Although polymer or latex *micro*particles have been thoroughly investigated with respect to protein adsorption,[19–21] there are very few studies of protein adsorption onto polymer *nano*particles, *e.g.*, a study of α-lactalbumin adsorbed onto 120 nm diameter polystyrene (PS) nanoparticles (NPs).[22]

Silica NPs have been the most commonly used NP in studies of surface-bound

* Address correspondence to dutcher@uoguelph.ca.

Received for review July 2, 2012 and accepted November 8, 2012.

Published online November 08, 2012
10.1021/nn302948d

proteins, including investigations of lysozyme,[9,12,23−25] BSA,[15,25−27] fibrinogen,[15] human carbonic anhydrase I (HCAI),[11] ribonuclease A,[28] hemoglobin,[26] and β-lactoglobulin (β-LG).[8] Soft, flexible proteins such as lysozyme, BSA, and hemoglobin undergo a partial loss of structure and a loss in enzyme activity when bound to SiO_2 NPs compared to their activity in solution, but lose more of their activity when bound to a flat SiO_2 surface. In general, these studies indicate that the smaller the NP, the closer the adsorbed protein is to its native state in solution,[11,12] presumably because the protein is locally exposed to a less denaturing surface area for very high curvatures.

Other surfaces with nanoscale curvature such as liposomes[29] and single-walled carbon nanotubes[30,31] have been investigated for their effect on the catalytic activity of enzymes. These measurements suggested that proteins can be stabilized on surfaces with nanoscale curvature more readily than on flat surfaces by suppressing unfavorable lateral protein−protein interactions. We hypothesize that surface curvature could also suppress *favorable* protein−protein interactions that hold together dimers and higher order oligomers. Testing this hypothesis is the goal of the present study.

Atomic force microscopy (AFM) has been used for over a decade to study protein unfolding at the single-molecule level,[32,33] and this is referred to as single-molecule force spectroscopy (SMFS). Protein molecules will attach spontaneously to an AFM tip that is brought into contact with a layer of adsorbed protein molecules, and the proteins can be unfolded by translating the tip away from the substrate while measuring the force experienced by the AFM tip (force−distance curve). This is the mechanical equivalent of chemical denaturation,[34] and this can be both reversible[35,36] and irreversible.[37] The pH-dependent transition between dimeric and monomeric forms of β-lactoglobulin has been studied using SMFS on a hydrophilic mica substrate,[38] and this was compared to the oligomerization behavior of β-LG on the hydrophobic surface of immobilized oil droplets.[39]

β-LG is an ideal protein for investigating interfacial phenomena. Although it is water-soluble, it adsorbs readily on both hydrophilic and hydrophobic surfaces.[19,38−40] The native environment of β-LG is at the oil−water interface in bovine milk, where it acts as an emulsifier. Its structure has been determined using X-ray crystallography[41,42] and NMR spectroscopy.[43,44] β-LG has a hydrophobic ligand-binding pocket[45] between two crossed beta-sheets (four strands each) with an α-helix and an additional β-strand on the external face. In solution, β-LG is composed of 15% α-helix, 50% β-sheet, and 30% random coil and has four of its five cysteine residues bound in disulfide bridges. Under physiological conditions, the ruminant variety of β-LG forms a dimer in solution, but dissociates into monomers below pH 3.[46]

In the present study, we have used SMFS to study changes in the lateral interactions between molecules of β-LG adsorbed onto hydrophobic solid substrates of well-defined nanoscale curvature. Capping of PS NP monolayers with an ultrathin PS film allowed us to obtain chemically pure, highly curved, hydrophobic PS surfaces that were stable in buffer. The samples contained regions of close-packed NP monolayers as well as bare flat regions, allowing for *in situ* comparisons of β-LG unfolding on curved and flat surfaces. SMFS measurements of β-LG adsorbed onto the PS NP surfaces exhibited well-defined peaks in the detachment length (L_c) distributions, which we identify as monomers and dimers of β-LG. We show that increasing the surface curvature, *i.e.*, using smaller PS NPs, results in fewer dimers of β-LG, demonstrating that protein−protein interactions are reduced significantly for highly curved surfaces. The results of the present study indicate that control of surface curvature provides a new method of modifying the interactions between adsorbed proteins, offering the possibility to spatially target native protein structures within cells and on biosensing surfaces.

RESULTS

A key step in the present study was the development of a protocol to fabricate highly curved, chemically pure, hydrophobic surfaces that are stable in buffer. This allowed SMFS experiments to be performed on proteins immobilized on surfaces under biologically relevant conditions. It was necessary to use hydrophobic PS NPs on a hydrophobic PS substrate so that water would be excluded from the NP-coated surface, since hydrophilic NPs or substrates would allow water to displace the NP film into the buffer. An added advantage of using hydrophobic surfaces in buffer is that these interfaces are analogous to the oil−water interface that is the native environment for β-LG molecules in bovine milk.

A schematic diagram of our sample preparation technique is shown in Figure 1 (for details, see the Methods section below). First, we spin-coated a thin (∼80 nm) film of pure, monodisperse PS onto a Si wafer to form a flat hydrophobic PS substrate. Next, we spin-coated a dilute aqueous suspension of surfactant-stabilized PS NPs onto the PS substrate. By adjusting the spin-coating conditions, it was possible to obtain regions that were coated by close-packed monolayers of the NPs, separated by bare regions of the underlying substrate.

Since the NP suspensions used in the present study are stabilized by surfactants, the surface chemistry of the NPs is necessarily different from that of pure PS. To produce chemically pure, highly curved surfaces, we used a water transfer procedure[47] to cap our PS NP surfaces with an ultrathin (10 nm thick) film of the same PS that was used to create the flat PS substrates

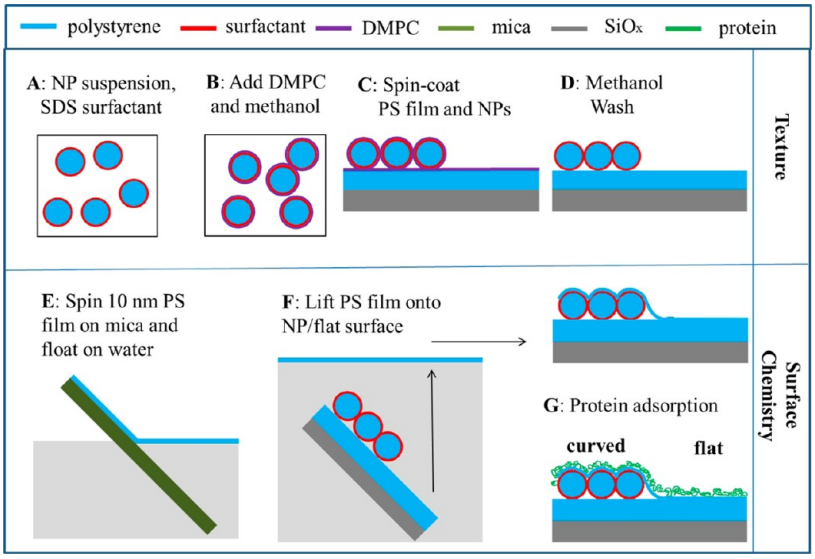

Figure 1. Schematic diagram of the sample preparation procedure. A surfactant-stabilized aqueous suspension of PS nanoparticles (NPs) (A) is mixed with DMPC and methanol (B) and then spin-coated onto a thin film of pure PS on Si (C), followed by a methanol rinse to remove the DMPC (D). This creates a textured surface with curved regions of NP monolayers and bare flat regions. To create a well-defined surface chemistry for this textured surface, we float a 10 nm thick film of pure PS film on mica (E) onto a clean water surface and capture this film onto the NP-coated substrates (F), capping the highly curved substrate with pure PS for use in the protein adsorption studies (G).

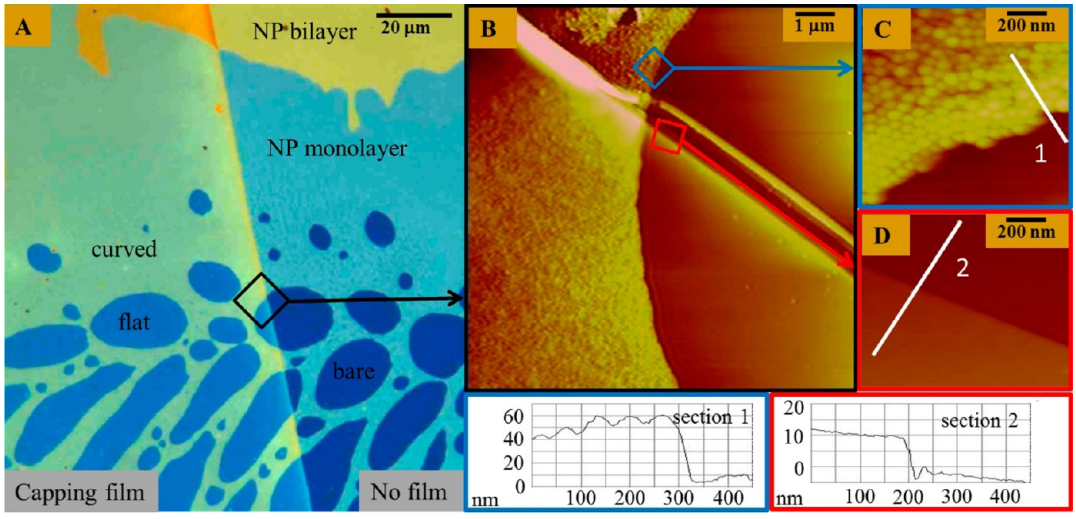

Figure 2. Reflected light optical microscopy (A) and atomic force microscopy (B–D) images of a 60 nm diameter NP film spin-coated onto a PS substrate and capped with a 10 nm thick PS film. Section 1 (corresponding to the white line in part (C)) shows the edge of the 60 nm diameter NP monolayer, in the absence of the capping film. Section 2 (corresponding to the white line in part (D)) shows the edge of the 10 nm thick PS capping film on a bare portion of the substrate.

(Figure 1: also see Methods). The transfer of the ultrathin PS film onto the top of the PS NP surface assured that the surfaces were chemically pure PS that was identical on the flat and curved regions of the samples, eliminating the effect of the ill-defined surface chemistry of the NPs. By choosing the thickness of the PS capping layer to be sufficiently small (10 nm thick) and by performing the water transfer procedure at an elevated temperature we ensured that the capping film would conform to the shape of the underlying NPs for NPs as small as 25 nm diameter.

The morphology of the PS-capped PS NP substrates was measured using both reflected light optical microscopy (OM) and atomic force microscopy, and representative images are shown in Figure 2. By carefully selecting the spin-coating conditions, it was possible to obtain NP-covered regions that contained well-ordered, close-packed monolayers of NPs perforated by large (mm-scale) holes, caused by dewetting of the water-based suspension during the spin-coating process. These holes exposed the flat PS substrate. We emphasize that although it may be possible to create NP films with more uniform coverage, the presence of highly curved and flat regions in the same microscopic domains allowed us to perform *in situ* comparisons using SMFS of proteins adsorbed to both curved and

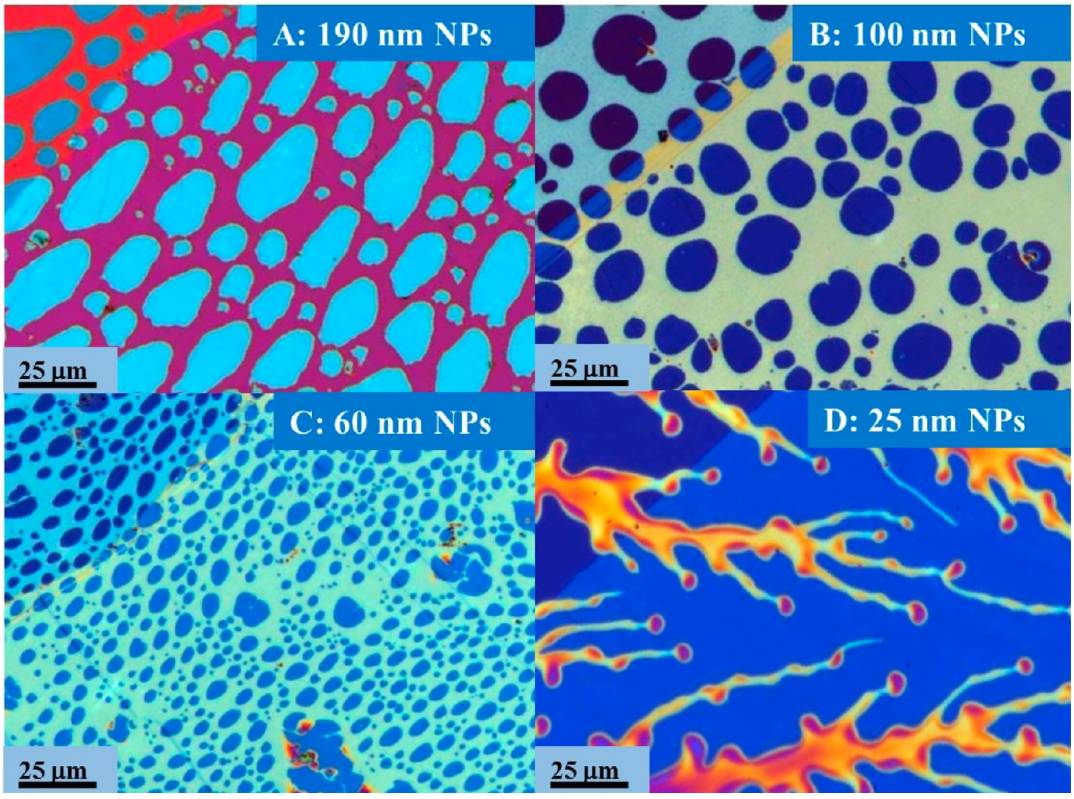

Figure 3. Reflected light optical microscopy images of PS-nanoparticle-coated substrates for 190 nm (A), 100 nm (B), 60 nm (C), and 25 nm (D) diameter NPs. PS NPs are spin-coated onto a ~80 nm thick PS film on Si (dark blue flat substrate in all images) and subsequently capped with a 10 nm thick PS film. The capping film produces a visible color change in both NPs and the PS substrate; regions of the sample not covered by the capping film are visible on the upper left in all images. The NPs assemble into web-like morphologies with a network of dewetting holes, for all but the 25 nm diameter NPs. Suspension concentration and spin speeds were chosen to yield films with approximately equal NP-covered and bare areas. The 25 nm diameter NPs have amorphous packing, but there are regions that approach monolayer thickness on the thinnest tendrils (as shown in the corresponding AFM images of these films in Figure 4).

flat surface topographies. The 10 nm thick PS capping film was clearly visible in the optical micrographs due to optical interference with the underlying film or NPs, which allowed us to target only the PS-capped surfaces for curved and flat regions in the AFM experiments.

OM images of the NP-film morphologies for NPs of different diameters are shown in Figure 3. During the spin-coating process, the 190, 100, and 60 nm diameter NPs self-assembled into films consisting of close-packed monolayer arrays of the NPs that were perforated with large dewetting holes, whereas the 25 nm diameter NPs formed frond-like tendrils that were separated by bare regions. In each of the OM images in Figure 3, the edge of the PS capping layer can be seen as a line in the upper left of the image, with the area covered by the capping layer extending to the lower right.

AFM topography images of the same NP films are shown in Figure 4. As in the OM images in Figure 3, the edge of the PS capping layer in each AFM image can be seen as a line in the upper left of the image, with the area covered by the capping layer extending to the lower right, with the PS capping film conforming around each of the NPs. The close-packed NP monolayers can be seen in Figure 4A, B, and C for the 190, 100, and 60 nm diameter NPs, whereas the 25 nm diameter NPs in Figure 4D form more disordered morphologies. Despite the disordered morphology of the 25 nm diameter NPs, isolated NPs projecting above the NP array can be identified, and these NPs were targeted for the SMFS measurements.

We alternately collected AFM images and SMFS data, which allowed us to target the tops of the NPs, with well-defined nanoscale curvatures, for SMFS measurements. For each sample, we collected hundreds of force–distance curves and used robust selection criteria (see Supporting Information) to select those curves that contained a well-defined worm-like chain (WLC) detachment peak (the last and longest peak in the force–distance curve). We then fit each of these selected curves to eq 1 (see Experimental Methods section below) to obtain the best-fit contour length (L_c) for the detachment peak. A representative force–distance curve with a WLC-like detachment peak is shown in Figure SI1 of the Supporting Information, together with a schematic diagram of the force spectroscopy measurement for a protein dimer.

In Figure 5A–D we show detachment length (L_c) histograms for the curved and flat regions of the 190,

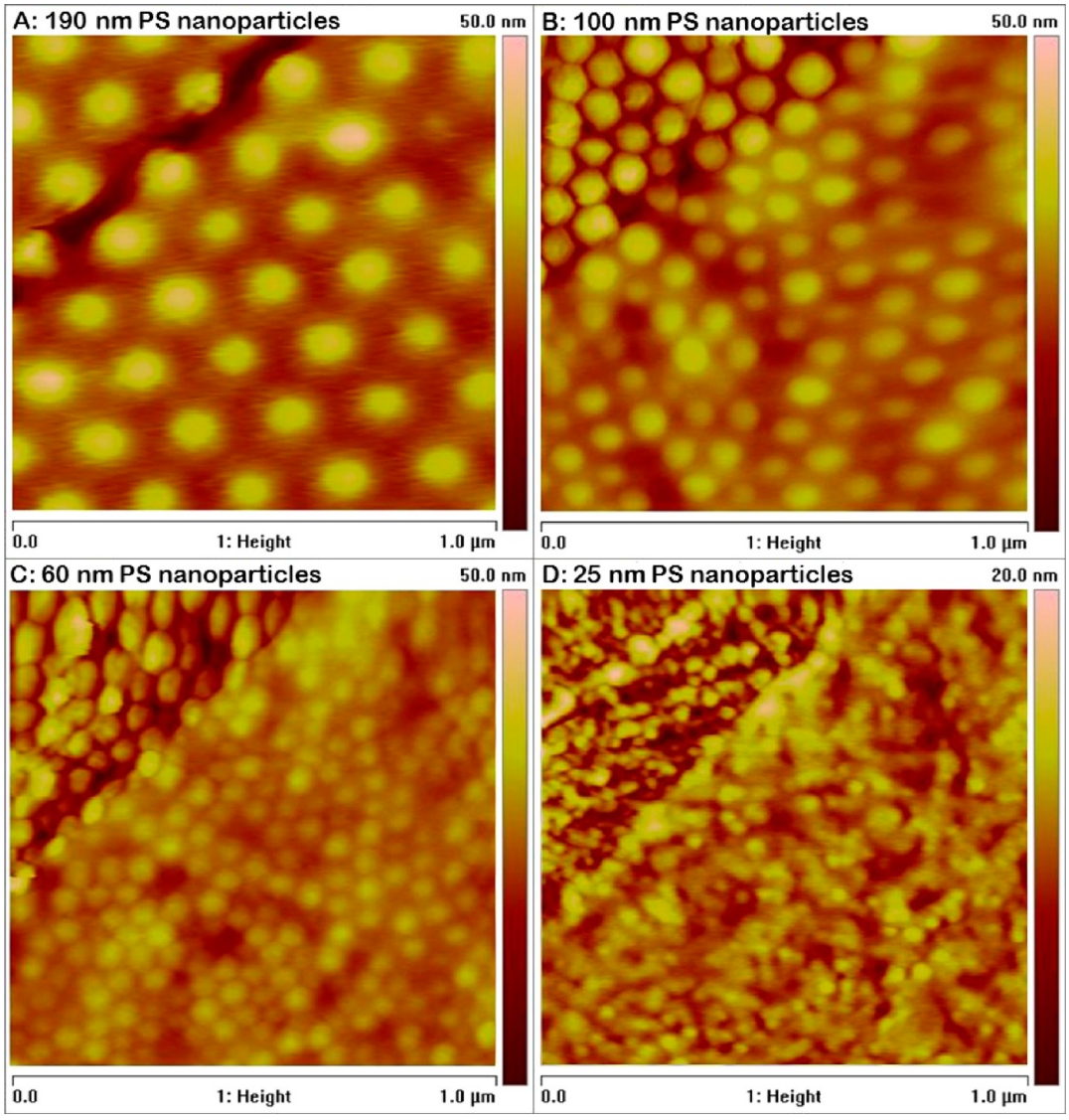

Figure 4. AFM topography images of NP-coated regions collected in fluid-phase contact mode. The images were collected at the edge of the 10 nm thick PS capping film, which covers the lower right of the images. The 190 nm (A), 100 nm (B), and 60 nm (C) diameter NPs formed close-packed monolayers with radii of curvature of 105, 60, and 40 nm, respectively, in the presence of the capping film. The packing of the 25 nm diameter NPs is disordered, but individual spheres that project above the neighboring spheres can be identified and targeted for SMFS experiments; in the presence of the capping film, the radius of curvature is 22 nm.

100, 60, and 25 nm diameter NP-coated samples. To facilitate comparisons between the different histograms, we have divided the number of counts in a given histogram by the total number N (shown in the legends of each plot) of the force–distance curves included in that histogram. Each histogram in Figure 5 includes data collected for between four and six different samples, with approximately fifty curves that satisfied our selection criteria obtained for each sample. By combining measurements of multiple samples with each NP diameter, we obtained excellent statistics for both the highly curved and bare flat surfaces obtained for each of the curved surfaces and the corresponding bare flat surfaces of the samples. In the Supporting Information, we show composite histograms of the detachment length (L_c) and the detachment force (F_d), in which the data correspond to all of the curves obtained for all of the bare flat surfaces. Since the contour length of a single β-LG molecule (monomer) is about 60 nm (162 amino acids $\times$ 0.36 nm/amino acid = 58.3 nm), detachment lengths longer than 60 nm indicate that the AFM tip has pulled on two or more proteins that are associated on the surface. There is no significant difference between the detachment length histograms for curved and flat surfaces for the 100 and 190 nm diameter NPs; the histograms show a dimer peak at 120 nm, which is about a quarter of the magnitude of the monomer peak near 60 nm. For the 60 nm diameter NPs, the dimer peak in the curved surface histogram is reduced with respect to that for

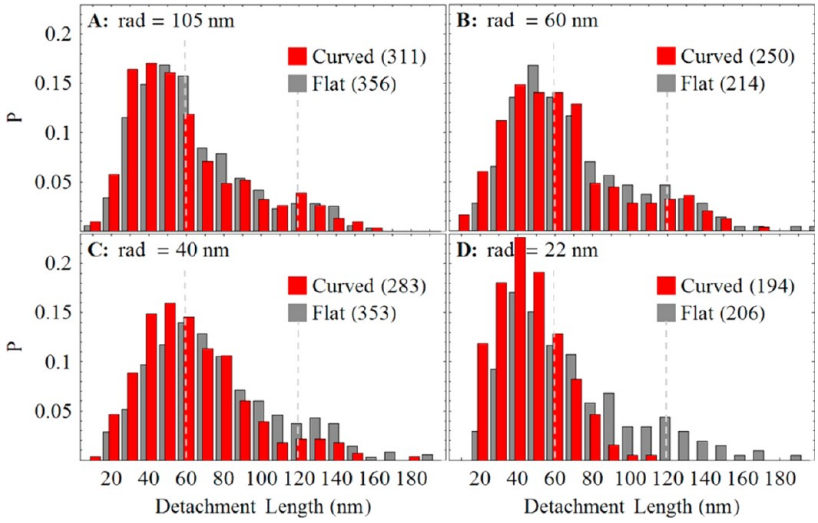

Figure 5. Histograms of the detachment length L_c for β-LG molecules on flat and curved regions of the surfaces of PS film-capped NP films for NPs of different diameters. On the vertical axis of each histogram, we have plotted the relative probability *P*, which is the number of counts divided by the total number *N* of the force–distance curves included in that histogram. The number of data points *N* included in each histogram is shown in brackets in the legend for each histogram. Both curved (red bars) and flat (gray bars) histograms are shown for PS-film-capped NPs, which have surfaces with radii of curvature of 105 nm (A), 60 nm (B), 40 nm (C), and 22 nm (D), respectively (NP diameter plus twice the capping film thickness, divided by 2). The vertical dotted lines correspond to the contour lengths of the β-LG monomers (58.3 nm) and dimers (117 nm). The bin width is 10 nm.

the flat surface, and for the 25 nm diameter NPs the dimer peak is not observed. Therefore, the number of dimers is significantly reduced on the most highly curved surface used in our experiment, demonstrating that the oligomerization of surface-bound proteins can be reduced by increasing the nanoscale curvature of the underlying substrate.

DISCUSSION

The importance of dimerization of proteins on surfaces has not been fully elucidated, and it is complicated by the additional influence of surface chemistry and surface forces. In the present study, we have chosen to study chemically identical flat and highly curved surfaces by creating surfaces that incorporate PS NP monolayers capped by a thin PS layer with intervening bare flat PS patches. This sample geometry has allowed us to focus exclusively on the geometric effect of surface curvature on oligomerization of surface-bound proteins. It is worth noting that surface curvature and roughness are not equivalent, since roughened surfaces span a wide range of curvatures. In contrast, by probing the tops of monodisperse NPs that are arranged in a close-packed array as in the present experiment, the local surface curvature has a very well-defined value. As a result, experiments on surfaces that are roughened on the nanoscale[48−50] cannot be compared directly with those performed on monodisperse NPs.

In addition, we have chosen to study the effect of surface curvature on a protein, β-LG, whose native state is at the oil–water interface in bovine milk. Most studies to date of adsorbed proteins have investigated globular proteins whose native state is in solution and which are denatured upon adsorption to a surface. Surface-active proteins would not be expected to follow the same trends: although BSA, a globular protein, was observed to become more ordered on smaller SiO_2 nanoparticles, fibrinogen, a surface-active protein, became less ordered.[15] These findings can be understood by taking into account the native environment of these proteins: BSA is a globular protein, and a highly curved surface pushes it toward the solvent state, whereas fibrinogen is a surface-active protein that requires lateral interactions to form fibrils.

Consideration of the environment of the protein is particularly relevant to our current investigation, since β-LG is found both in aqueous solution and at the surface of oil droplets in oil–water emulsions. While β-LG is known to form a dimer in solution, its structure on a hydrophobic surface is not known. A previous study from our laboratory compared the detachment lengths of β-LG on a hydrophilic mica surface with that on a hydrophobic liquid oil droplet.[39] On the hydrophilic surface, for which β-LG is expected to have a conformation that is similar to that in solution, a peak at 120 nm was observed in the detachment length histogram that was roughly equal in magnitude to the monomer peak at 60 nm, indicating a significant presence of surface-bound dimers. For β-LG bound to oil droplets, the dimer peak was present but considerably smaller in the detachment length histograms, indicating a smaller fraction of dimers on the hydrophobic surface. The distributions of detachment lengths observed in the current study on

flat PS are similar to that measured on the oil droplet, which gives us confidence that the hydrophobic solid PS substrates used in the present study are analogous to the hydrophobic liquid oil surface, which is the native environment for β-LG in milk. However, we note that the presence of a small dimer peak in the detachment length histograms for the flat hydrophobic surface makes it challenging to measure changes in this peak with increasing surface curvature.

In the detachment length histograms shown in Figure 5, a large, well-defined peak in each distribution occurs at a detachment length of 40−50 nm, which we attribute to isolated β-LG monomers on the surface, with no significant differences between the position of this peak for the flat and curved surfaces. The difference between this peak position and the contour length of a single β-LG molecule (58.3 nm) is likely due to the nonspecific interaction between the AFM tip and the β-LG molecules, since it is expected that the AFM tip will sample attachment points near the middle of the molecule more often than at the end of the molecule, and this leads to detachment lengths that are, in general, less than the full contour length of the extended molecule. The second peak in the detachment length distribution occurs at the value of 110−120 nm. This peak position agrees quite closely with the contour length for two β-LG molecules attached end-to-end. We attribute this peak predominantly to dimers of β-LG, as in our previous studies.[38,39] Our interpretation of the measured contour lengths is straightforward: if the measured contour lengths are longer than the contour length of a monomer, they correspond to oligomers. We stress that we make no assumptions about changes to the secondary or tertiary structure of the β-LG molecules due to adsorption, but we make conclusions only about changes to the oligomerization of the molecules, as measured in the SMFS experiments. To demonstrate the convergence of our statistical sampling, in Figure SI2 (see Supporting Information) we present a composite L_c histogram for 1128 force−distance curves collected on the bare flat PS regions of all of the samples used in the present study, which clearly shows the same features as in each histogram obtained for the flat bare PS surfaces in Figure 5. Figure SI2 also shows a composite histogram of detachment forces (F_d) for all bare flat PS surfaces, which contains a well-defined peak at $F_d \approx 150$ pN and a significant tail to larger F_d values.

As the surface curvature is increased, we observe a decrease in the number of dimers present on the highly curved surfaces, such that only monomers are observed for the surfaces incorporating the smallest NPs with a diameter of 25 nm. To interpret these results, we first consider changes in the dimerization of β-LG molecules upon adsorption to a hydrophobic surface. In solution at neutral pH, the β-LG molecules exist as dimers. Upon adsorption onto a flat hydrophobic surface, there is a significant reduction in the population of dimers. This can be seen from our SMFS measurements for β-LG molecules on both large oil droplets[39] and flat PS (the present study), for which we observe a significant reduction in the population of β-LG dimers relative to the relatively large population of β-LG dimers observed on a hydrophilic mica surface.[38] This disruption of dimers upon adsorption to a flat hydrophobic surface likely occurs during the significant rearrangement of each of the β-LG molecules, as they expose their hydrophobic pockets to the underlying hydrophobic surface. The effect of increasing surface curvature in the present study seems to further disrupt the dimerization of β-LG since each adsorbed molecule has more available space and therefore fewer tendencies to interact with neighboring molecules relative to its local environment on a flat surface. This is observed as the disappearance of the dimer peak in the contour length (L_c) histogram for the surfaces with the highest curvature. Since the size of the protein molecules is small compared to the diameter of even the smallest NPs, it is likely that the surface coverage of β-LG molecules is comparable on NPs of different diameters and that the dominant effect with decreasing NP diameter is weakened lateral interactions between adsorbed proteins. This result is important since the oligomerization state of a protein often modulates its function. Because of this, our results may have interesting biotechnological applications, especially in the context of solid-state devices, since it may be possible to tailor surface topography to invoke biological function.

The results of the present study also have direct implications for biological systems. Oligomerization of proteins occurs commonly in biology, which suggests that it is a significant molecular control mechanism in biochemical signaling. In particular, dimerization is a common regulatory mechanism in signal transduction, catalyzing reactions by bringing substrates and active sites together in favorable orientations and enhancing specificity by means of increasing the effective surface area.[51] Dimerization occurs in many cell surface receptors, where ligand-induced dimerization at the extracellular domain triggers kinase activity in the cytoplasm, which triggers cell response.[52,53] Homo- and heterodimers often exhibit different biological activity than their constituent monomers, and the monomer−dimer transition may provide a dynamic trigger for biochemical cascades, can facilitate chemical modifications, and can provide temporary storage or stability for the active monomer pool.[54] Models have also suggested that the fast-binding equilibrium of dimerization reactions can lower the noise in a biochemical network by absorbing fluctuations and buffering

against sudden changes in monomer copy number. Thus dimerization can reduce the noise in the physiologically relevant long-time regime by shifting it to shorter times that do not propagate to the level of gene activation and transcription.[55]

The possibility of manipulating oligomerization is of great interest for medical and biotechnological applications since the functional state of a protein is often determined by its oligomerization state. In pharmaceutical preparations, chemical additives and cosolvents can be used to stabilize or compete with interprotein contacts,[56] or oligomerization can be controlled by alterations of the primary sequence that target the protein coupling interface.[56,57] For example, the dimerization interface of β-LG is strongly influenced by the charged attraction of Asp33 on one monomer and Arg40 on the other; changing one of these residues to an amino acid of the opposite charge (D33R or R40D/E) strongly inhibits dimerization.[58] However, these methods are not appropriate *in vivo* since they lack the ability to target a specific protein population without changing the global chemical environment or altering the protein at the genetic level. Using substrate curvature to control oligomerization, as demonstrated in the present study, offers the possibility of spatially targeting native protein structures within cells and on biosensing surfaces.

SUMMARY AND CONCLUSIONS

We have fabricated surfaces with uniform nanoscale surface curvature that are stable in aqueous buffer, and we have used SMFS to study the lateral interactions between molecules of the surface-active protein β-LG. By capping our NP-coated surfaces with a very thin pure PS film, we have eliminated the effect of the ill-defined surface chemistry of the NPs, allowing us to perform a controlled study of the effect of high surface curvature on adsorbed proteins. This is an important result since all NPs must be stabilized with surfactant (or charge) in suspension, thereby contaminating the surface of interest in suspension-based studies of NP−protein interactions. We have measured the distribution of detachment lengths for β-LG on NPs of different diameters, and we have found that, for the most highly curved surfaces, it differs from that measured on a flat surface on the same sample: there is a lower incidence of detachment lengths that are longer than the contour length of a monomer for the curved surface. We conclude that a highly curved surface reduces the lateral interactions between adsorbed β-LG proteins, favoring the monomer form of the protein.

EXPERIMENTAL METHODS

A 1.5% (by mass) solution of polystyrene (PS, Polymer Source, M_w/M_n = 1.12, M_w = 675 000) in toluene was spin-coated at 1500 rpm onto a 1 cm × 1 cm oxidized Si(100) wafer and annealed for 18 h at 105 °C under an oil-free vacuum. The thickness of the resulting films was between 70 and 80 nm, as measured by ellipsometry and AFM. The resulting hydrophobic surface was then used as a substrate to spin-coat PS nanoparticles.

Suspensions of PS NPs (Bangs Laboratories) of four different diameters (25, 60, 100, and 190 nm) were purchased with a concentration of 10% by mass. The 25 nm diameter NPs were spin-coated directly from this stock suspension. All other NP suspensions were diluted to 1% by mass with Milli-Q water, then mixed in a 1:1 ratio with a solution of 400 parts methanol to 1 part dimeristoyl phosphatidylcholine (DMPC) by mass (Avanti, lyophilized powder). The DMPC acted as a surfactant to allow 60, 100, and 190 nm diameter NP suspensions to wet the hydrophobic PS film substrate with a much lower contact angle than the pure aqueous suspensions, allowing for convective self-assembly of NPs at the evaporative front during spin-coating. The stock 25 nm diameter NP suspension had a much lower contact angle than the others, and we hypothesize that the 25 nm diameter NPs are small enough to act as their own surfactant, as in Pickering emulsions. After spin-coating, all samples were flushed thoroughly with methanol to dissolve the DMPC and then dried in clean nitrogen gas, including the 25 nm diameter NP samples to which DMPC was not added.

For the capping film, a 0.25% (by mass) solution of PS (Polymer Source, M_w/M_n = 1.12, M_w = 675 000) in toluene was spin-coated at 2000 rpm onto a freshly cleaved 2 cm × 10 cm piece of muscovite mica and annealed for 18 h at 105 °C under an oil-free vacuum. The resulting film was 10 nm thick, as measured using AFM (see Figure 2). A razor blade was used to score this film into a grid of twenty 1 cm^2 squares. The film-coated mica was then lowered at a 45° angle into a pool of Milli-Q water at 70 °C. Since mica is hydrophilic and PS is hydrophobic, the PS film floats onto the water surface. After 1 min of thermal equilibration under water, the 1 cm^2 Si-PS-NP-PS substrates were lifted at an angle of ~30° under a piece of floating PS film to transfer the PS film onto the solid substrate. Samples were put under vacuum for 1 h to remove water and then stored in air. Although the conformation of the PS film around the highly curved NPs was not consistent for all samples or regions of one sample, it was always possible to identify (using AFM imaging) regions with sufficient conformation of the PS film around the NPs for SMFS measurements.

The morphology of the PS-NP-PS substrates was measured using both reflected light optical microscopy and atomic force microscopy. The OM measurements were performed using an Olympus BX-60 microscope using bright-field illumination. The AFM measurements were performed in contact mode in liquid using a Veeco Multimode AFM with a Nanoscope IV controller. Nanoworld PNP-TR triangular cantilevers with a nominal tip radius of curvature of 10 nm and a spring constant of 0.08 nN/nm were used. The spring constant for each tip was measured *in situ* using the thermal tuning method, and results were always within 20% of the nominal value. The deflection sensitivity was also measured for each tip (~45 V/nm), and the resulting force exerted on the surface during imaging was always <2 nN. Images were typically collected using a lateral range of 1−2 μm using a scan rate of 1−1.5 Hz, resulting in a tip speed of <5 μm/s.

A 1% solution (by mass) of β-LG (Sigma-Aldrich, variant A) in 20 mM imidazole buffer (pH = 6.8) was prepared and stored at 4 °C overnight. After warming to room temperature, 20 μL of the protein solution was deposited onto the PS-NP-PS substrates and allowed to incubate for 1 h. Excess liquid was then removed from the substrate by wicking with a Kimwipe tissue, and the substrate was rinsed repeatedly (3×) with imidazole buffer,

leaving only adsorbed protein on the substrate. The sample was then inserted into an AFM fluid cell and allowed to equilibrate for 30 min before measurement using atomic force microscopy.

The protein layers on the PS-NP-PS substrates were measured with AFM in contact mode in liquid for both imaging and force spectroscopy measurements. A new AFM cantilever was used for each curved and flat surface within a single experiment. For AFM imaging of the protein layers, we used the same operating parameters as for imaging the PS-NP-PS substrates. For the force spectroscopy experiments, a vertical range of 400 nm and a tip speed of 775 nm/s were used, with a 2 s wait time at the surface.

We note that although the hydrophobic interaction of 25, 60, and 100 nm diameter NPs was strong enough to adhere them to the PS substrate, the mechanical perturbation associated with AFM contact imaging was enough to dislodge some of the 190 nm diameter NPs if they were not covered with the capping film. Hence the capping film also served to mechanically stabilize the adhesion of the 190 nm diameter NPs, and this made AFM imaging and targeted force spectroscopy measurements of the proteins possible. A slow aging process for the capping film was also observed, with the PS film conforming completely around the largest NPs after ~2 months, which eliminated the flat areas of stretched film between NPs that are apparent in Figure 3. The Digital Instruments Nanoscope "Point-and-Shoot" software module (Bruker AXS) was used to image a region of the NP monolayer and target the top of NPs that had six close-packed neighbors. Typically ~100 force–distance curves were collected per NP, with a ~10% success rate for protein attachment. Because the AFM tip diameter is comparable to or less than the diameter of the NPs on our textured surfaces and we target the top of a given spherical NP for the SMFS measurements, there is little chance of contacting the surface of a neighboring NP. To ensure this in the presence of a small amount of lateral drift of the AFM system, no NP was probed for more than 2–3 min. Approximately 10 NPs were probed for each AFM image, and 3–5 images were collected at different parts of the sample, for both curved and flat surfaces. This resulted in 300–500 curves for both curved and flat surfaces per sample, of which one-quarter to one-third contained a well-defined worm-like chain curve (see eq 1 below) at detachment and were used for further data analysis (see Supporting Information). Four or five experiments were performed for each size of NP, resulting in ~300 curves per flat and curved data set. In half of the experiments, force spectroscopy measurements were performed on the curved surface first and then on the flat surface, reversing this order in the other half of the experiments, to ensure that aging of the protein layer did not affect our observations. Since it was necessary to image NPs before performing the force spectroscopy measurement on the protein layer, flat areas were also scanned with a similar force before performing the force spectroscopy measurements so that all protein molecules were treated in a similar fashion on both flat and curved surfaces.

An objective, automated method was developed to identify and analyze force–distance curves that contained a well-behaved detachment peak (see Supporting Information for details). The criteria for deciding whether or not to include a given curve in the detachment length (L_c) histogram were as follows: the data points in the detachment peak had a maximum force that was larger than 50 pN; the maximum force occurred at an AFM tip–sample separation greater than 5 nm; the data points beyond the detachment peak in the curve corresponded to a flat baseline with near-zero force, and the data points within the detachment peak tracked continuously to the baseline and were well-described by the worm-like chain function:[59]

$$\frac{FL_p}{k_BT} = \frac{1}{4}\left[1 - \frac{x}{L_c}\right]^{-2} - \frac{1}{4} + \frac{x}{L_c} \qquad (1)$$

where F is the measured force, x is the tip–sample separation, T is temperature, k_B is Boltzmann's constant, and L_p is the persistence length of the chain (fixed at a value of 0.4 nm, which is typical for proteins). The best fit value of the detachment length (L_c) was obtained by fitting the detachment peak data to eq 1.

Conflict of Interest: The authors declare no competing financial interest.

Acknowledgment. The authors gratefully acknowledge fruitful discussions with Dr. K. Dalnoki-Veress, financial support from the Natural Sciences and Engineering Research Council of Canada for a Discovery Grant to J.R.D., and the Canada Foundation for Innovation and the Ontario Research Fund for research infrastructure. J.R.D. acknowledges support from the Canada Research Chairs (CRC) program.

Supporting Information Available: Further details are provided concerning the fitting criteria that were used for analyzing the single-molecule force spectroscopy data, and composite histograms for the bare flat PS surfaces are shown. This material is available free of charge *via* the Internet at http://pubs.acs.org.

REFERENCES AND NOTES

1. Ozin, G. A.; Arsenault, A. C.; Cademartiri, L. *Nanochemistry: A Chemical Approach to Nanomaterials*, 2nd ed.; Royal Society of Chemistry: Cambridge, UK, 2009.
2. Nam, J. M.; Thaxton, C. S.; Mirkin, C. A. Nanoparticle-Based Bio-Bar Codes for the Ultrasensitive Detection of Proteins. *Science* **2003**, *301*, 1884–1886.
3. Reynolds, R. A. I.; Mirkin, C. A.; Letsinger, R. L. Homogeneous, Nanoparticle-Based Quantitative Colorimetric Detection of Oligonucleotides. *J. Am. Chem. Soc.* **2000**, *122*, 3795–3796.
4. Brigger, I.; Dubernet, C.; Couvreur, P. Nanoparticles in Cancer Therapy and Diagnosis. *Adv. Drug Delivery Rev.* **2002**, *54*, 631–651.
5. LaVan, D. A.; Lynn, D. M.; Langer, R. Moving Smaller in Drug Discovery and Delivery. *Nat. Rev. Drug Discovery* **2002**, *1*, 77–84.
6. Neimeyer, C. M. Nanoparticles, Proteins, and Nucleic Acids: Biotechnology Meets Materials Science. *Angew. Chem., Int. Ed.* **2001**, *40*, 4128–4158.
7. Santos, A. M.; Fedorov, A.; Martinho, J. M. G.; Baptista, R. P.; Angela Taipa, M.; Cabral, J. M. S. Orientation of Cutinase Adsorbed onto PMMA Nanoparticles Probed by Tryptophan Fluorescence. *J. Phys. Chem. B* **2008**, *112*, 3581–3585.
8. Wu, X.; Narsimhan, G. Characterization of Secondary and Tertiary Conformational Changes of β-Lactoglobulin Adsorbed on Silica Nanoparticle Surfaces. *Langmuir* **2008**, *24*, 4989–4998.
9. Billsten, P.; Wahlgren, M.; Arnebrant, T.; McGuire, J.; Elwing, H. Structural Changes of T4 Lysozyme upon Adsorption to Silica Nanoparticles Measured by Circular Dichroism. *J. Colloid Interface Sci.* **1995**, *175*, 77–82.
10. Jiang, X.; Jiang, J.; Jin, Y.; Wang, E.; Dong, S. Effect of Colloidal Gold Size on the Conformational Changes of Adsorbed Cytochrome *c*: Probing by Circular Dichroism, UV-Visible, and Infrared Spectroscopy. *Biomacromolecules* **2005**, *6*, 46–53.
11. Lundqvist, M.; Sethson, I.; Jonsson, B.-H. Protein Adsorption onto Silica Nanoparticles: Conformational Changes Depend on the Particles' Curvature and the Protein Stability. *Langmuir* **2004**, *20*, 10639–10647.
12. Vertegel, A. A.; Siegel, R. W.; Dordick, J. S. Silica Nanoparticle Size Influences the Structure and Enzymatic Activity of Adsorbed Lysozyme. *Langmuir* **2004**, *20*, 6800–6807.
13. Ravindran, A.; Singh, A.; Raichur, A. M.; Chandrasekaran, N.; Mukherjee, A. Studies on Interaction of Colloidal Ag Nanoparticles with Bovine Serum Albumin (BSA). *Colloids Surf., B* **2010**, *76*, 32–37.
14. Yokoyama, K.; Welchons, D. R. The Conjugation of Amyloid Beta Protein on the Gold Colloidal Nanoparticles' Surfaces. *Nanotechnology* **2007**, *18*, 1–7.
15. Roach, P.; Farrar, D.; Perry, C. C. Surface Tailoring for Controlled Protein Adsorption: Effect of Topography at the Nanometer Scale and Chemistry. *J. Am. Chem. Soc.* **2006**, *128*, 3939–3945.
16. Teichroeb, J. H.; Forrest, J. A.; Jones, L. W. Anomalous Thermal Denaturing of Proteins Adsorbed to Nanoparticles. *Eur. Phys. J. E* **2006**, *21*, 19–24.

17. Teichroeb, J. H.; Forrest, J. A.; Jones, L. W. Size-Dependent Denaturing Kinetics of Bovine Serum Albumin Adsorbed onto Gold Nanospheres. *Eur. Phys. J. E* **2008**, *26*, 411–415.
18. Wu, W.-H.; Sun, X.; Yu, Y.-P.; Hu, J.; Zhao, L.; Liu, Q.; Zhao, Y.-F.; Li, Y.-M. TiO_2 Nanoparticles Promote β-Amyloid Fibrillation *in vitro*. *Biochem. Biophys. Res. Commun.* **2008**, *373*, 315–318.
19. Caldwell, K. D.; Li, J.; Li, J.-T.; Dalgleish, D. G. Adsorption Behavior of Milk Proteins on Polystyrene Latex. A Study Based on Sedimentation Field-Flow Fractionation and Dynamic Light Scattering. *J. Chromatogr.* **1992**, *604*, 63–71.
20. Norde, W.; Gonzalez, F. G.; Haynes, C. A. Protein Adsorption on Polystyrene Latex Particles. *Polym. Adv. Technol.* **1995**, *6*, 518–525.
21. Tan, J. S.; Martic, P. A. Protein Adsorption and Conformational Change on Small Polymer Particles. *J. Colloid Interface Sci.* **1990**, *136*, 415–431.
22. Engel, M.; Visser, A.; van Mierlo, C. Conformation and Orientation of a Protein Folding Intermediate Trapped By Adsorption. *Proc. Natl. Acad. Sci. U. S. A.* **2004**, *101*, 11316–11321.
23. Bower, C. K.; Sananikone, S.; Bothwell, M. K.; McGuire, J. Activity Losses Among T4 Lysozyme Charge Variants after Adsorption to Colloidal Silica. *Biotechnol. Bioeng.* **1999**, *64*, 373–376.
24. Czeslik, C.; Winter, R. Effect of Temperature on the Conformation of Lysozyme Adsorbed to Silica Particles. *Phys. Chem. Chem. Phys.* **2001**, *3*, 235–239.
25. Norde, W.; Anusiem, A. C. I. Adsorption, Desorption and Re-Adsorption of Proteins on Solid Surfaces. *Colloids Surf.* **1992**, *66*, 73–80.
26. Kondo, A.; Oku, S.; Higashitani, K. Structural Changes in Protein Molecules Adsorbed on Ultrafine Silica Particles. *J. Colloid Interface Sci.* **1991**, *143*, 214–221.
27. Larsericsdotter, H.; Oscarsson, S.; Buijs, J. Structure, Stability and Orientation of BSA Adsorbed to Silica. *J. Colloid Interface Sci.* **2005**, *289*, 26–35.
28. Shang, W.; Nuffer, J. H.; Dordick, J. S.; Siegel, R. W. Unfolding of Ribonuclease A on Silica Nanoparticle Surfaces. *Nano Lett.* **2007**, *7*, 1991–1995.
29. Litt, J.; Padala, C.; Asuri, P.; Vutukuru, S.; Athmakuri, K.; Kumar, S.; Dordick, J. S.; Kane, R. S. Enhancing Protein Stability by Adsorption onto Raftlike Lipid Domains. *J. Am. Chem. Soc.* **2009**, *131*, 7107–7111.
30. Asuri, P.; Karajanagi, S. S.; Yang, H.; Yim, T.-J.; Kane, R. S.; Dordick, J. S. Increasing Protein Stability through Control of the Nanoscale Environment. *Langmuir* **2006**, *22*, 5833–5836.
31. Karajanagi, S. S.; Vertegel, A. A.; Kane, R. S.; Dordick, J. S. Structure and Function of Enzymes Adsorbed onto Single-Walled Carbon Nanotubes. *Langmuir* **2004**, *20*, 11594–11599.
32. Engel, A.; Muller, D. J. Observing Single Biomolecules at Work with the Atomic Force Microscope. *Nat. Struct. Biol.* **2000**, *7*, 715–718.
33. Fisher, T. E.; Oberhauser, A. F.; Carrion-Vazquez, M.; Marszalek, P. E.; Fernandez, J. M. The Study of Protein Mechanics with the Atomic Force Microscope. *Trends Biochem. Sci.* **1999**, *24*, 379–384.
34. Carrion-Vazquez, M.; Oberhauser, A. F.; Fowler, S. B.; Marszalek, P. E.; Broedel, S. E.; Clarke, J.; Fernandez, J. M. Mechanical and Chemical Unfolding of a Single Protein: A Comparison. *Proc. Natl. Acad. Sci. U. S. A.* **1999**, *96*, 3694–3699.
35. Marszalek, P. E.; Lu, H.; Li, H.; Carrion-Vazquez, M.; Oberhauser, A. F.; Schulten, K.; Fernandez, J. M. Mechanical Unfolding Intermediates in Titin Modules. *Nature* **1999**, *402*, 100–103.
36. Rief, M.; Gautel, M.; Oesterhelt, F.; Fernandez, J. M.; Gaub, H. E. Reversible Unfolding of Individual Titin Immunoglobulin Domains by AFM. *Science* **1997**, *276*, 1109–1112.
37. Brockwell, D. J.; Beddard, G. S.; Paci, E.; West, D. K.; Olmsted, P. D.; Smith, D. A.; Radford, S. E. Mechanically Unfolding the Small, Topologically Simple Protein L. *Biophys. J.* **2005**, *89*, 506–519.
38. Touhami, A.; Dutcher, J. R. pH-Induced Changes in Adsorbed β-Lactoglobulin Molecules Measured using Atomic Force Microscopy. *Soft Matter* **2009**, *5*, 220–227.
39. Touhami, A.; Alexander, M.; Kurylowicz, M.; Gram, C.; Corredig, M.; Dutcher, J. R. Probing Protein Conformations at the Oil Droplet-Water Interface Using Single-Molecule Force Spectroscopy. *Soft Matter* **2011**, *7*, 10274–10284.
40. Elofsson, U. M.; Paulsson, M. A.; Arnebrant, T. Adsorption of β-Lactoglobulin A and B in Relation to Self-Association: Effect of Concentration and pH. *Langmuir* **1997**, *13*, 1695–1700.
41. Brownlow, S.; Morais Cabral, J. H.; Cooper, R.; Flower, D. R.; Yewdall, S. J.; Polikarpov, I.; North, A. C. T.; Sawyer, L. Bovine β-Lactoglobulin at 1.8 Å Resolution -- Still an Enigmatic Lipocalin. *Structure* **1997**, *5*, 481–495.
42. Qin, B. Y.; Bewley, M. C.; Creamer, L. K.; Baker, H. M.; Baker, E. N.; Jameson, G. B. Structural Basis of the Tanford Transition of Bovine β-Lactoglobulin. *Biochemistry* **1998**, *37*, 14014–14023.
43. Kuwata, K.; Hoshino, M.; Forge, V.; Era, S.; Batt, C. A.; Goto, Y. Solution Structure and Dynamics of Bovine β-Lactoglobulin A. *Protein Sci.* **1999**, *8*, 2541–2545.
44. Uhrinova, S.; Smith, M. H.; Jameson, G. B.; Uhrin, D.; Sawyer, L.; Barlow, P. N. Structural Changes Accompanying pH-Induced Dissociation of the β-Lactoglobulin Dimer. *Biochemistry* **2000**, *39*, 3565–3574.
45. Sawyer, L.; Kontopidis, G. The Core Lipocalin, Bovine β-Lactoglobulin. *Biochim. Biophys. Acta* **2000**, *1482*, 136–148.
46. Townend, R.; Weinberger, L.; Timasheff, S. N. Molecular Interactions in β-Lactoglobulin. IV. The Dissociation of β-Lactoglobulin below pH 3.5. *J. Am. Chem. Soc.* **1959**, *82*, 3175–3179.
47. Forrest, J. A.; Rowat, A. C.; Dalnoki-Veress, K.; Stevens, J. R.; Dutcher, J. R. Brillouin Light Scattering Studies of the Mechanical Properties of Polystyrene/Polyisoprene Multilayered Thin Films. *J. Polym. Sci., Part B: Polym. Phys* **1996**, *34*, 3009–3016.
48. Cai, K.; Bossert, J.; Jandt, K. D. Does the Nanometre Scale Topography of Titanium Influence Protein Adsorption and Cell Proliferation? *Colloids Surf., B* **2006**, *49*, 136–144.
49. Dolatshahi-Pirouz, A.; Rechendorff, K.; Hovgaard, M. B.; Foss, M.; Chevallier, J.; Besenbacher, F. Bovine Serum Albumin Adsorption on Nano-Rough Platinum Surfaces Studied by QCM-D. *Colloids Surf., B* **2008**, *66*, 53–59.
50. Rechendorff, K.; Hovgaard, M. B.; Foss, M.; Zhdanov, V. P.; Besenbacher, F. Enhancement of Protein Adsorption Induced by Surface Roughness. *Langmuir* **2006**, *22*, 10885–10888.
51. Klemm, J. D.; Schreiber, S. L.; Crabtree, G. R. Dimerization as a Regulatory Mechanism in Signal Transduction. *Annu. Rev. Immunol.* **1998**, *16*, 569–92.
52. Bouvier, M. Oligomerization of G-Protein-Coupled Transmitter Receptors. *Nat. Rev. Neurosci.* **2001**, *2*, 274–286.
53. Heldin, C.-K. Dimerization of Cell Surface Receptors in Signal Transduction. *Cell* **1995**, *80*, 213–223.
54. Nooren, I. M. A.; Thornton, J. M. Structural Characterisation and Functional Significance of Transient Protein-Protein Interactions. *J. Mol. Biol.* **2003**, *325*, 991–1018.
55. Ghim, C.-M.; Almaas, E. Genetic Noise Control *via* Protein Oligomerization. *BMC Syst. Biol.* **2008**, *2*, 94.
56. Schein, C. H. Controlling Oligomerization of Pharmaceutical Proteins. *Pharm. Acta Helv.* **1994**, *69*, 119–126.
57. Hashimoto, K.; Panchenko, A. R. Mechanisms of Protein Oligomerization, the Critical Role of Insertions and Deletions in Maintaining Different Oligomeric States. *Proc. Natl. Acad. Sci. U. S. A.* **2010**, *107*, 20352–20357.
58. Sakurai, K.; Goto, Y. Manipulating Monomer-Dimer Equilibrium of Bovine β-Lactoglobulin by Amino Acid Substitution. *J. Biol. Chem.* **2002**, *277*, 25735–25740.
59. Bustamante, C.; Marko, J. F.; Siggia, E. D.; Smith, S. Entropic Elasticity of λ-Phage DNA. *Science* **1994**, *271*, 1599–1600.